JPET Fast Forward. Published on March 24, 2006 as DOI: 10.1124/jpet.105.095711

JPET #95711

Physiological and Biophysical Factors that Influence Alzheimer's Disease Amyloid Plaque Targeting of Native and Putrescine Modified Human Amyloid β 40

Karunya K. Kandimalla*, Geoffry L. Curran, Silvina S. Holasek, Emily J. Gilles, Thomas M. Wengenack, Marina Ramirez-Alvarado, and Joseph F. Poduslo

Molecular Neurobiology Laboratory

Departments of Neurology, Neuroscience, and Biochemistry/Molecular Biology (*KK, GC, SH, EG, TW, JP*), Department of Biochemistry/Molecular Biology (MRA)

Mayo Clinic College of Medicine, Rochester, MN 55905

Running title: Amyloid plaque targeting of AB40 in Alzheimer's disease

Corresponding author: Joseph F. Poduslo

Address: Mayo Clinic College of Medicine, 200 First Street SW, Rochester, MN55905

Phone: (507) 284 1784

Fax: (507) 284 3383

Email: poduslo.joseph@mayo.edu

Number of text pages: 22

Number of tables: 1

Number of figures: 10

Number of references: 22

Number of words in the abstract: 248

Number of words in the introduction: 620

Number of words in the discussion: 1393

Abbreviations:

AD, Alzheimer's disease; Aβ40, unlabeled amyloid beta 40; ^{125}I-Aβ40, amyloid beta 40 labeled with ^{125}I; APP, amyloid precursor protein; PS1, presenilin 1; WT, wild type; BBB, blood brain barrier; CSF, cerebrospinal fluid; IV, intravenous; BSA, bovine serum albumin; BCA, Bicinchoninic acid protein assay reagent ; TCA, trichloroacetic acid; V_p, residual brain region plasma volume; PS, cerebrovascular permeability coefficient-surface area product ; KRB, Kreb's Ringer bicarbonate buffer; DMEM, Dulbecco's modified eagle medium; 2,4-DNP, 2,4-dinitrophenol; V_{ss}, steady state volume of distribution; AUC, area under the plasma concentration curve; Cl, clearance.

Section option: Absorption, Distribution, Metabolism & Excretion

JPET Fast Forward. Published on March 24, 2006 as DOI: 10.1124/jpet.105.095711
This article has not been copyedited and formatted. The final version may differ from this version.

ABSTRACT

Amyloid β40 (Aβ40) and its derivatives are being developed as probes for the ante-mortem diagnosis of Alzheimer's disease (AD). Putrescine-Aβ40 (PUT-Aβ40) showed better plaque targeting than the native Aβ40, which was not solely explained by the differences in their blood-brain-barrier (BBB) permeabilities. The objective of this study was to elucidate the physiological and biophysical factors influencing the differential targeting of Aβ40 and PUT-Aβ40. Despite better plaque targeting ability, ^{125}I-PUT-Aβ40 was more rapidly cleared from the systemic circulation than ^{125}I-Aβ40 following IV administration in mice. The BBB permeability of both compounds was inhibited by circulating peripheral Aβ40 levels. ^{125}I-Aβ40 but not ^{125}I-PUT-Aβ40 was actively taken up by the mouse brain slices in-vitro. Only Fluorescein-Aβ40 and not Fluorescein-PUT-Aβ40 was localized in the brain parenchymal cells in-vitro. The metabolism of ^{125}I-Aβ40 in the brain slices was twice as great as ^{125}I-PUT-Aβ40. ^{125}I-Aβ40 efflux from the brain slices was saturable and found to be five times greater than that of ^{125}I-PUT-Aβ40. Thioflavin-T fibrillogenesis assay demonstrated that PUT-Aβ40 has a greater propensity to form insoluble fibrils compared to Aβ40, most likely due to the ability of PUT-Aβ40 to form β sheet structure more readily than Aβ40. These results demonstrate that the inadequate plaque targeting of Aβ40 is due to cellular uptake, metabolism, and efflux from the brain parenchyma. Despite better plaque targeting of PUT-Aβ40, its propensity to form fibrils may render it less suitable for human use and thus allow increased focus on the development of novel derivatives of Aβ with improved characteristics.

JPET Fast Forward. Published on March 24, 2006 as DOI: 10.1124/jpet.105.095711
This article has not been copyedited and formatted. The final version may differ from this version.

INTRODUCTION

Amyloid β (Aβ) protein is a hydrophobic peptide that is thought to be neurotoxic. A consensus is emerging that Aβ proteins, as soluble monomers or polymers, play a critical role in the neurotoxicity and subsequent development of amyloid plaque formation which contributes to the pathology of Alzheimer's disease (AD). The extracellular accumulation of Aβ peptides into plaques is one of the pathological hallmarks for the definitive post-mortem diagnosis of AD. A diagnostic imaging technique capable of directly visualizing these amyloid plaques will provide not only a more definitive premortem diagnosis of AD, but also a tool for prognostication and evaluation of putative therapies (Poduslo et al., 2002).

Currently, no method exists to image "individual" amyloid plaques in humans for a definitive and early diagnosis of AD. Radiolabeled molecular probes that bind to β-amyloid plaques have recently been demonstrated both *in vitro* and in animal studies (Skovronsky et al., 2000; Wengenack et al., 2000a; Agdeppa et al., 2001; Bacskai et al., 2001). The most notable of these probes is the Pittsburgh compound-B, which allowed the researchers to visualize amyloid plaques by bulk tissue enhancement after PET imaging for the first time in AD patients (Klunk et al., 2004). While scintigraphic imaging of β-amyloid plaques is promising, certain difficulties may be envisioned for clinical application. The most obvious is poor spatial resolution. The spatial resolution of clinically available tomographic scintigraphic techniques (positron emission tomography or single-photon emission computed tomography) is several times poorer than that of standard 3D magnetic resonance imaging (MRI).

The ability of human Aβ40 and PUT-Aβ40 to selectively target amyloid plaques in AD transgenic mouse (APP,PS1) brain has provided an opportunity to use them as molecular probes to image amyloid plaques with MRI. ^{125}I-Aβ40 was reported to have high in vitro binding affinity to the amyloid plaques in human and APP,PS1 mouse brain slices and high in vivo permeability at the BBB (Zlokovic et al., 1993; Maness et al., 1994; Poduslo et al., 1997; Poduslo et al., 1999; Mackic et al., 2002); however, the plaque targeting ability of ^{125}I-Aβ40 following IV injection in AD transgenic mice was low (Wengenack et al., 2000a). The putrescine modified Aβ40 (PUT-Aβ40) was shown to have two fold higher BBB permeability than unmodified Aβ40 and was able to target and label amyloid plaques in APP,PS1 animals following intravenous administration. When covalently linked to gadolinium diethylenetriaminepentaacetic acid (Gd-DTPA), which provides contrast for MRI imaging, Gd-PUT-Aβ40 was able to provide enough contrast to image amyloid plaques in APP,PS1 mice while Gd-Aβ40 failed to provide the required contrast (Poduslo et al., 2002). The differences in the efficacy of these compounds to label plaques ex-vivo cannot be completely explained by the differences in their permeability values at the BBB.

Permeability at the blood-brain-barrier (BBB), endothelial transcytosis, as well as diffusion within and efflux from the brain parenchyma are important factors that determine the amount of Aβ-probe available to target plaques. The proportion of Aβ-probe in the extracellular space of the brain parenchyma versus intracellular uptake is another important consideration that will determine the successful targeting of amyloid plaques. Adequate knowledge of the transport kinetics of human Aβ protein and its

derivatives at the BBB and in the brain will allow us to design smart molecular probes capable of labeling plaques in Alzheimer's patients, as well as provide further information regarding the dynamics of Aβ transport in the progression of AD.

The objective of the current study is to investigate various factors affecting the 1) in vivo uptake of Aβ40 and PUT- Aβ40 at the BBB; 2) accumulation within and efflux from the brain tissue in vitro; and 3) binding to the amyloid plaques, as a means to explain the better targeting ability of PUT- Aβ40 over native Aβ40.

MATERIALS AND METHODS

Synthesis of human Aβ40.

Aβ40 was synthesized on an ABI 433 peptide synthesizer (Foster City, CA) using HBTU activation and the manufacturer's suggested synthesis protocols. The starting resin was Val-NovaSyn TGA resin (Calbiochem-Novabiochem, San Diego, CA). The peptides were cleaved from the solid support using 5% crystalline phenol, 5% water, 2.5% triisopropylsilane and 87.5% TFA for two hours at room temperature and were purified by reverse-phase HPLC using a heated 250 x 21.2 mm C18 Jupiter column (Phenomonex Corp). The weights of the peptides were confirmed by electrospray ionization mass spectrometry (Sciex API 165).

Synthesis of fluorescein labeled Aβ40 (F-Aβ40). After the final deprotection of the N-terminal Fmoc group, the peptide resin was washed with 12% diisopropylethylamine/dichloromethane (DIEA/DCM). A two equivalent excess of NHS-

fluorescein (Pierce, Rockford, IL) was dissolved in 6 ml of dimethylformamide (DMF) and added to the resin saturated with 12% DIEA/DCM. The resin slurry was mixed overnight at room temperature, followed by several washes with DMF and DCM. The success of the fluorescein addition was confirmed by a negative ninhydrin reaction.

Putrescine modification of Aβ40 and F-Aβ40. Putrescine modification of synthetic human Aβ40 and F-Aβ40 was performed by covalent linkage of the polyamine to carboxylic acid groups using carbodimide at pH of 6.7 as described previously (Poduslo and Curran, 1996a; Poduslo and Curran, 1996b)

Radioiodination of proteins. A 500 µg of Human Aβ40 or PUT- Aβ40 was labeled with carrier-free $Na^{125}I$, whereas the bovine serum albumin (BSA) (500 µg) was labeled with carrier-free $Na^{131}I$ using the chloramine-T procedure as described previously (Poduslo et al., 2001). Free radioactive iodine was separated from the radiolabeled protein by dialysis against 0.01 M phosphate buffered saline at pH 7.4 (Sigma-Aldrich Co., St. Louis, MO). Purity of the radiolabeled proteins was determined by trichloroacetic acid (TCA) precipitation. The radiolabeled protein was considered to be acceptable if the precipitable radioactive counts were greater than 95% of the total counts. The specific activity of the proteins thus obtained was determined as 2.0 ± 0.1 µCi/µg. No significant difference was observed between the specific activities of ^{125}I-Aβ40 and ^{125}I-PUT-Aβ40.

Animals. Wild type (WT mice (B6/SJL strain) were obtained from the Jackson Laboratory (Bar Harbor, ME). The mice were housed in a virus-free barrier facility under a 12-hr light/dark cycle, with ad libitum access to food and water. All the experimental procedures were performed in accordance with the NIH Guide for the Care and Use of Laboratory Animals using protocols approved by the Mayo Institutional Animal Care and Use Committee.

PUT-Aβ40 pharmacokinetics studies., Before the beginning of the experiment, the femoral vein and the femoral artery of each mouse were catheterized under general anesthesia (Poduslo et al., 2001). An IV bolus dose of ^{125}I-PUT-Aβ40 (100 µCi in 100 µl) was administered through the femoral vein. Blood samples (20 µl) were obtained from the femoral artery at 0.25, 1, 3, 5, 10 and 15 min intervals. At the end of the experiment, an IV bolus dose of ^{131}I-BSA (100 µCi in 100 µl) was administered to serve as a measure of residual plasma volume (V_p). One minute following the ^{131}I-BSA injection, the final blood sample was collected, and the animal was sacrificed. The blood samples were diluted to a volume of 100 µl using normal saline, centrifuged, and the supernatant was obtained. Following TCA precipitation, the supernatant was assayed for ^{125}I and ^{131}I radioactivity in a two-channel gamma counter (Cobra II, Packard). The measured activity was corrected for the background and crossover of ^{131}I activity into the ^{125}I channel. At the end of the experiment, the brain of the animal was removed from the cranial cavity, dissected into cortex, caudate putamen, hippocampus, thalamus, brain stem, and cerebellum, and assayed for ^{125}I and ^{131}I radioactivity. The effect of Aβ40 on the ^{125}I-PUT-Aβ40 uptake at the blood brain barrier was determined by both

co-administering and sequential administration of 1 mg of unlabelled Aβ40 with 100 µCi of ^{125}I-PUT-Aβ40.

Metabolism of ^{125}I-PUT-Aβ40. The metabolism of ^{125}I-PUT-Aβ40 in the plasma of WT mice was determined by adding 0.1 µCi of ^{125}I-PUT-Aβ40 to 350 µl of plasma. A 20 µl sample was taken from the mixture at regular intervals up to 60 min and the amount of intact ^{125}I-PUT-Aβ40 in the sample was determined by TCA precipitation. The metabolism of ^{125}I-PUT-Aβ40 in the presence of brain, liver, kidney and spleen slices was determined using the organs obtained from WT mice following perfusion with PBS. The organs were weighed, chopped into 1mm thick slices using a tissue slicer (Stoelting Co. Wood Dale, IL) and placed in oxygenated (95% O_2 and 5%CO_2) KRB until the start of the experiment. The tissue slices were then transferred to 5 ml of KRB containing 0.1 µCi of ^{125}I-PUT-Aβ40 and incubated at 37^{o}C under 5% CO_2 for the entire length of the experiment. Samples (20 µl) of the medium were obtained at regular intervals and assayed for the intact protein by TCA precipitation.

Brain Slices. After sacrificing with an overdose of sodium pentobarbital (200 mg/kg, IP), the animals were decapitated and the brains were carefully removed from the cranial cavity. Each brain was cut coronally into 1 mm thick slices containing cortex and hippocampus. The slices were placed in oxygenated (95% O_2 and 5%CO_2) KRB until the start of the experiment.

Brain slice uptake of ^{125}I-Aβ40 and ^{125}I-PUT-Aβ40

JPET Fast Forward. Published on March 24, 2006 as DOI: 10.1124/jpet.105.095711
This article has not been copyedited and formatted. The final version may differ from this version.

Effect of time. Following the equilibration in KRB, each brain slice was incubated in 1 ml of donor solution containing ^{125}I- Aβ40 (0.8 µCi/ml of KRB) at 37^{o}C. The brain slices were sampled at different time points (0, 10, 15, 30, 45, and 60 min), rinsed with KRB, and assayed for ^{125}I radioactivity in a two-channel gamma counter (Cobra II, Packard).

Effect of donor concentration. Following the equilibration, each brain slice was incubated at 37^{o}C in a 1 ml donor solution containing different concentrations of ^{125}I-Aβ40 (0.05-28.4 µCi/ ml of KRB). After 15 min, the brain slices were removed from the donor solutions, rinsed with KRB, and assayed for radioactivity using a dual channel gamma counter.

Effects of metabolic inhibitors. Following the equilibration, brain slices was pre-incubated with the metabolic inhibitors ouabain (1mM) or 2,4-dinitrophenol(2,4-DNP) (1mM) for 30 minutes. Each brain slice was then transferred to 1 ml donor solution (pre-incubate + 0.6 µCi/1 ml of ^{125}I-Aβ40 or PUT-Aβ40) maintained at 37^{o}C. After 15 min, the brain slices were removed, rinsed with KRB, and assayed for radioactivity in a two-channel gamma counter.

Cellular accumulation of F-Aβ40 and F-PUT-Aβ40 in the brain parenchyma. Each brain slice was incubated in 1 ml of donor solution containing F-Aβ40 or F-PUT-Aβ40 (40 µg/ml of KRB) at 37 ^{o}C. After 15 min, the slice was removed from the donor solution, placed on a cover slip moistened with KRB and imaged under a Zeiss LSM 410 (Carl Zeiss, Thornwood, NY) laser confocal microscope

^{125}I-Aβ40 and ^{125}I-PUT-Aβ40 efflux from brain slices.

JPET Fast Forward. Published on March 24, 2006 as DOI: 10.1124/jpet.105.095711
This article has not been copyedited and formatted. The final version may differ from this version.

WT mice brain slices were equilibrated in KRB for 15 min at 37^{o}C. Each slice was then incubated in a 1 ml donor solution containing various concentrations of ^{125}I-Aβ40 or ^{125}I-PUT-Aβ40 at 37^{o}C for 30 minutes, washed with KRB and incubated in 5 ml of KRB (receiving medium). The brain slices were harvested at various time points: 0, 10, 15 and 30 min, rinsed with KRB and assayed for ^{125}I radioactivity. The initial rates of efflux (<15 min) of these compounds from the brain slices were calculated at various donor concentrations. The rates of efflux were normalized by the donor concentrations and plotted against log donor concentrations.

Aβ40 and PUT-Aβ40 fibril formation. Thioflavin T (THT) is a fluorescent dye that exhibits substantial enhancement in the fluorescence intensity upon binding to amyloid fibrils. Due to an excellent correlation between the THT fluorescence and the amount of amyloid fibrils, THT fibrillogenesis assay is widely used to quantify the amyloid fibril formation. In the current study, Aβ40 and PUT-Aβ40 fibril formation kinetics were followed using THT fibrillogenesis assay, which is detailed as follows: Aβ40 and PUT-Aβ40 were incubated at 37^{o}C in TRIS-EDTA buffer (50mM Tris, 5mM EDTA and 150 mM NaCl) under continuous shaking (200 rpm) for 24 hours. A 60 µl aliquot of the reaction mixture was obtained at 0, 1, 2, 4, 6, 9, 12, 24, 48, 90 and 120 hrs, mixed with 1.2 ml of 5 µM Thioflavin T (THT) in TRIS-EDTA and assayed for fluorescence (excitation λ = 450 nm and emission λ = 480 nm). The fluorescence intensity of each compound was normalized with the maximal fluorescence value of the compound and plotted against time.

Circular Dichroism (CD) Spectorscopy. The secondary structures of Aβ40 and PUT-Aβ40 were determined using CD spectroscopy. A 20 µM solution of each protein was prepared in PBS (pH = 7.2), filtered using 0.22 µm syringe filter, and transferred to a 0.2 cm path length quartz cuvette. The CD spectra of Aβ40 and PUT-Aβ40 were obtained from 260-200 nm at 4 ^{o}C, scanning every 1 nm with an averaging time of 5 sec, on an AVIV CD spectrometer Model 215 (AVIV Instruments).

Data Analysis. The ^{125}I-PUT-Aβ40 plasma concentration profile following the single intravenous bolus dose of ^{125}I-Aβ40 was best described by a biexponential disposition function $C(t) = Ae^{-\alpha t} + Be^{-\beta t}$, where C(t) = ^{125}I-PUT-Aβ40 / ml of plasma, A and B are the intercepts and α and β are the slopes of the biexponential curve. Pharmacokinetic parameters were estimated by nonlinear curve fitting using Gauss-Newton (Levenberg and Hartley) algorithm and iterative reweighting (WinNonlin® Professional, version 4.1, Mountain view, CA). Secondary parameters such as the C_{max} (maximum plasma concentration), the first ($t_{1/2(\alpha)}$) and the second ($t_{1/2(\beta)}$) phase half-lives, the plasma clearance (Cl), the steady-state volume of distribution (V_{ss}), and area under the plasma concentration curve (AUC) were also calculated using WinNonlin. The mean values of controls and treatments were compared by Student's t-test using GraphPad Prism version 4.0 (GraphPad Software, San Diego California USA).

PS and V_p measurements were calculated as described previously by Poduslo (1993). The residual brain region plasma volume (V_p, µl/g) is calculated as

JPET Fast Forward. Published on March 24, 2006 as DOI: 10.1124/jpet.105.095711
This article has not been copyedited and formatted. The final version may differ from this version.

$$V_p = \frac{q_p \times 10^3}{C_v \times WR}, \quad \text{Eqn. 1}$$

where q_p is the radioactivity (cpm) of ^{131}I-BSA present in the tissue. C_v is the ^{131}I-BSA concentration (cpm/ml) in plasma, W is the dry weight (g) of the brain region, and R is the wet weight / dry weight ratio for mice of a defined age group. From the total ^{125}I-Aβ40 content (q_T) (cpm) of the brain region, the amount of ^{125}I-Aβ40 that enters the brain region extravascular space (q) (cpm/g) is calculated as

$$q = \frac{q_T}{WR} - \frac{V_p C_a}{10^3}, \quad \text{Eqn. 2}$$

where C_a is the final ^{125}I-Aβ40 concentration (cpm/ml) in plasma. The PS (ml/g/s) of the BBB is calculated as

$$PS = \frac{q(t)}{\int_0^t C_p dt}, \quad \text{Eqn. 3}$$

where t is the circulation time, q(t) is the extravascular ^{125}I activity in the brain region at time t, and $\int_0^t C_p dt$ is the plasma concentration time integral of ^{125}I-Aβ40.

The initial rates of efflux of ^{125}I-Aβ40 and ^{125}I-PUT-Aβ40 from the WT brain slices were normalized by the donor concentrations and plotted against log donor concentrations (log C). The inhibitory concentrations (IC_{50}) of ^{125}I-Aβ40 efflux from the brain slices in vitro was determined by fitting the following equation to the data using GraphPad Prism version 3.03 (GraphPad Software, San Diego, CA).

$$NE = NE_{min} + \frac{(NE_{max} - NE_{min})}{1 + 10^{(\log C - \log IC50)}} \quad \text{Eqn. 4}$$

JPET Fast Forward. Published on March 24, 2006 as DOI: 10.1124/jpet.105.095711
This article has not been copyedited and formatted. The final version may differ from this version.

where NE_{max} is the maximum normalized efflux value, which was obtained at the lowest ^{125}I-Aβ40 concentration. NE_{min} is the minimum NE value obtained at the highest ^{125}I-Aβ40 concentration.

RESULTS

The in vivo targeting abilities of molecular probes may be compromised due to: 1) rapid elimination from the systemic circulation; 2) competitive inhibition by high circulating Aβ levels in APP,PS1 mice; 3) proteolytic degradation in the brain parenchyma; 4) uptake and degradation by neurons; and 5) efflux from the brain. In this study, we systematically studied and compared the influence of each of the above factors on the amyloid plaque targeting of Aβ40 and PUT-Aβ40.

^{125}I-PUT-Aβ40 plasma pharmacokinetics. Upon IV administration, the ^{125}I-PUT-Aβ40 concentrations in the plasma of WT mice declined rapidly exhibiting a bi-exponential disposition with short α and β half-lives ($t_{1/2\ (\alpha)}$ and $t_{1/2\ (\beta)}$, respectively) (Figure 1, Table 1). The C_{max}, $t_{1/2(\alpha)}$ and AUC were significantly lower, whereas the clearance (Cl) and steady state volume of distribution (V_{ss}) was significantly higher for ^{125}I-PUT-Aβ40 compared to previously reported values for ^{125}I-Aβ40 (Kandimalla et al., 2005). These differences are mostly likely due to rapid clearance normally observed for cationized proteins (Dellian et al., 2000) or significantly higher metabolism of ^{125}I-PUT-Aβ40 in the peripheral tissues compared to that of ^{125}I-Aβ40.

JPET Fast Forward. Published on March 24, 2006 as DOI: 10.1124/jpet.105.095711
This article has not been copyedited and formatted. The final version may differ from this version.

^{125}I-PUT-Aβ40 metabolism in the peripheral tissues. To investigate the contribution of peripheral tissue metabolism on the rapid elimination of ^{125}I-PUT-Aβ40 from the systemic circulation, in vitro degradation of ^{125}I-PUT-Aβ40 in the presence of WT mice tissue slices (liver, kidney and spleen) as well as plasma was studied. Although ^{125}I-PUT-Aβ40 degradation in the WT plasma was slightly higher than the degradation in DMEM, not more than 10% of the initial amount of ^{125}I-PUT-Aβ40 was degraded in 60 min (Figure 2). The degradation of ^{125}I-PUT-Aβ40 in the presence of liver slices was similar to that of ^{125}I-Aβ40, with substantial degradation in 60 min. The extent of ^{125}I-PUT-Aβ40 degradation in the kidney and spleen was significantly lower compared to that of ^{125}I-Aβ40 (Figure 2). These results demonstrate that despite rapid clearance from the peripheral circulation compared to ^{125}I-Aβ40, the metabolism of ^{125}I-PUT-Aβ40 in the peripheral organs of elimination was significantly lower than that of ^{125}I-Aβ40.

^{125}I-Aβ40 Brain Uptake. It has been established in our earlier studies that the PS value, which is a measure of BBB permeability of a protein, of ^{125}I-PUT-Aβ40 is significantly higher than that of ^{125}I-Aβ40 in APP,PS1 mice (Wengenack et al., 2000a). These transgenic mice develop distinct plaques at the age of 3 months with substantial amyloid burden by 6 months, mostly in the cortex and hippocampus (Wengenack et al., 2000) and carry significantly higher levels of Aβ40 (13.9 pmol/ml) in the peripheral circulation compared to WT mice (2.9 pmol/ml) at 6 months (Poduslo et al., 2001). It was shown that the plaque burden in APP,PS1 animals increases linearly with age (Wengenack et al., 2000b), and the endogenous Aβ40 levels in the peripheral circulation are expected to follow a similar trend. The efficacy of PUT-Aβ40 to target

JPET Fast Forward. Published on March 24, 2006 as DOI: 10.1124/jpet.105.095711
This article has not been copyedited and formatted. The final version may differ from this version.

plaques in older APP,PS1 animals with high endogenous levels of Aβ40 may be compromised if Aβ40 competes with PUT-Aβ40 for the BBB uptake. Hence it is important to determine if Aβ40 can competitively inhibit the PUT-Aβ40 absorption at the BBB. It was observed that when 1 mg of Aβ40 was co-administered with 100 µCi of ^{125}I-PUT-Aβ40, the PS values of ^{125}I-PUT-Aβ40 decreased significantly in various brain regions (Figure 3). The V_p values, however, did not change significantly due to the co-administration of unlabeled Aβ40 (Figure 3). To verify that the reduction in the PS values was not due to change in the pharmacokinetics of ^{125}I-PUT-Aβ40 resulting from a possible interaction with unlabeled Aβ40 in the syringe prior to injection, the PS values were determined by first injecting 1 mg of unlabeled Aβ40 immediately followed by 100 µCi of ^{125}I-PUT-Aβ40. The PS values of ^{125}I-PUT-Aβ40 obtained from this experiment were not significantly different from the PS values obtained when ^{125}I-PUT-Aβ40 was co-administered with Aβ40 (data not shown). These results demonstrate that the endogenous Aβ40 levels in the peripheral circulation can reduce the permeability of ^{125}I-PUT-Aβ40 as well as ^{125}I-Aβ40 (Kandimalla et al., 2005) at the BBB.

Brain slice uptake studies. After permeating the BBB, ^{125}I-Aβ40 or ^{125}I-PUT-Aβ40 must diffuse across the brain parenchyma to reach the plaque sites. The relative diffusivities of ^{125}I-Aβ40 and ^{125}I-PUT-Aβ40 across the brain parenchyma may be directly related to their plaque targeting capabilities. Hence the uptake of ^{125}I-Aβ40 and ^{125}I-PUT-Aβ40 into WT mouse brain slices was determined in vitro.

Effect of time. The uptake of ^{125}I-Aβ40 into WT mouse brain slices was linear till 15 min and reached a plateau from 15 to 60 min (Figure 4).

Effect of donor concentration. Uptake of ^{125}I-Aβ40 across the WT mouse brain slices was non-linearly dependent upon the donor concentration (Figure 5). Upon fitting a Michaelis-Menten type expression to the data, the K_m and V_{max} were estimated to be 18.4 μCi/ml and 2622 nCi/g wet weight, respectively, whereas 24.8 nCi/g wet weight was estimated to be non-specifically bound to the tissue.

Localization of Fluorescein labeled Aβ40 (F-Aβ40) and PUT- Aβ40 (F-PUT-Aβ40) in the brain parenchyma. A laser confocal micrograph of WT brain slice incubated with F-Aβ40 demonstrated intense fluorescence accumulated in the cells, most likely neurons, of cortex with faint background fluorescence (Figure 6). Laser confocal micrograph of F-PUT-Aβ40 demonstrated numerous dark spots amidst intensely fluorescent background in the cortex. These results suggest that F-PUT-Aβ40 was not taken up by the cells and remained in the extracellular space of the brain parenchyma (Figure 6).

Effects of metabolic inhibitors. The uptake of ^{125}I-Aβ40 in the WT brain slices treated with metabolic inhibitors such as ouabain (ATPase inhibitor) or 2,4-DNP (uncoupler of oxidative phosphorylation) was reduced significantly compared to the untreated brain slices (Figure 7), suggesting that the brain slice uptake of ^{125}I-Aβ40 is energy dependent and carrier mediated. The uptake of ^{125}I-PUT-Aβ40 in the WT brain slices was not significantly affected in the presence of a metabolic inhibitor such as 2,4-DNP (Figure

JPET Fast Forward. Published on March 24, 2006 as DOI: 10.1124/jpet.105.095711
This article has not been copyedited and formatted. The final version may differ from this version.

7). Hence the uptake of ^{125}I-PUT-Aβ40 in the brain slices is more likely by passive diffusion.

^{125}I-Aβ40 and ^{125}I-PUT-Aβ40 efflux from brain slices.

As indicated above and from earlier studies conducted in our lab, Aβ40 efflux from WT brain slices could be inhibited by 2,4-DNP, which strongly suggested that it is a carrier mediated process (Kandimalla et al., 2005). In the next experiment, we evaluated the saturability of ^{125}I-Aβ40 efflux process and compared it with that of ^{125}I-PUT-Aβ40 (Figure 8). The initial rates of ^{125}I-Aβ40 efflux from WT brain slices, normalized with the donor concentration, decreased with an increase in log donor concentration. In contrast, the normalized initial rates of ^{125}I-PUT-Aβ40 efflux from WT brain slices did not change appreciably with log donor concentration. These results demonstrated that the efflux of ^{125}I-Aβ40 from WT brain slices is carrier mediated, whereas the efflux of ^{125}I-PUT-Aβ40 is predominantly by passive diffusion.

Biophysical characterization of Aβ40 and PUT-Aβ40

Circular Dichroism (CD) spectra: The CD spectra of Aβ40 and PUT-Aβ40 illustrated in Figure 9 demonstrate that Aβ40 has a random coil structure, whereas PUT-Aβ40 assumes a β-sheet structure in phosphate buffered saline (pH = 7.2) at 4^{o}C .

Kinetics of fibril formation: It is believed that high concentration of soluble Aβ accumulates over time in the brain extracellular space, polymerizes into insoluble fibrils, and eventually forms amyloid plaques. The ease with which a molecule can form fibrils

is considered a direct measure of its likelihood to provide a seed for plaque formation. The ideal diagnostic probe would not form fibrils after reaching the brain parenchyma, but only bind to pre-existing plaques. We studied the fibril formation of Aβ40 and PUT-Aβ40 using Thioflavin-T (THT) assay (Levine, 1993). THT binds to the β-sheet structure of fibrils and emits fluorescence. The intensity of the fluorescence provides a direct measure of the extent of fibril formation. The intensity of THT fluorescence plotted against time in Figure 10 describes the kinetics of Aβ40 and PUT-Aβ40 fibril formation. Aβ40 forms fibrils with a lag time of 2 hrs, whereas PUT-Aβ40 forms fibrils readily. Moreover, the extent of fibril formation with PUT-Aβ40 was substantially higher than Aβ40 reflected in the larger fluorescence intensity. At the end of the experiment, the fibril formation was verified by electron microscopy (data not shown).

DISCUSSION

^{125}I-Aβ40 and ^{125}I-PUT-Aβ40 have demonstrated a differential ability to target amyloid plaques in APP,PS1 transgenic mice after intravenous injection. As a result, they are utilized in this study as model compounds to investigate various physiological factors (plasma clearance, BBB permeability, parenchymal diffusion and metabolism, and efflux from the CNS) and biophysical factors (effect of charge, ability to form fibrils, and affinity to plaques) that affect plaque targeting.

It is generally believed that lower plasma clearance resulting in high sustained plasma levels of the probe will enhance its BBB permeability. Our earlier studies demonstrated that ^{125}I-Aβ40 is rapidly eliminated from the systemic circulation due to significant renal

clearance and hepatic metabolism (Kandimalla et al., 2005). Despite better plaque targeting ability, ^{125}I-PUT-Aβ40 is more rapidly cleared from the systemic circulation than ^{125}I-Aβ40 following IV administration. Unlike ^{125}I-Aβ40, the rapid clearance of ^{125}I-PUT-Aβ40 did not correlate with its metabolism in the peripheral tissues such as liver, kidney and spleen. While the metabolism of ^{125}I-PUT-Aβ40 in the liver slices was only slightly lower compared to ^{125}I-Aβ40, its metabolism in kidney slices was significantly lower than ^{125}I-Aβ40. Since the molecular size of ^{125}I-PUT-Aβ40 or ^{125}I-Aβ40 is small, these molecules can be eliminated by the kidney without the need for initial catabolism in the liver. Moreover, the microvascular permeability of cationized proteins like ^{125}I-PUT-Aβ40 was found to be substantially higher than the native proteins (Dellian et al., 2000), resulting in their increased renal clearance. Although, higher microvascular permeability can increase the distribution of ^{125}I-PUT-Aβ40 to brain (Poduslo 1996b), increase in the renal clearance and rapid distribution to peripheral tissues could diminish the net effect. Hence, it is unlikely that the better plaque targeting ability of ^{125}I-PUT-Aβ40 compared to ^{125}I-Aβ40 is due to favorable plasma pharmacokinetics.

Like the BBB permeability of ^{125}I-Aβ40, which decreased significantly in the presence of unlabeled Aβ40 (0.125 mg–2 mg) in a dose dependent manner(Kandimalla et al., 2005), the BBB permeability of ^{125}I-PUT-Aβ40 decreased when co-administered with 1 mg of Aβ40. Even though the PS value of ^{125}I-PUT-Aβ40 is higher than that of ^{125}I-Aβ40 in WT mice, the PS value of ^{125}I-PUT-Aβ40 co-administered with 1 mg of Aβ40 was similar to the PS value of ^{125}I-Aβ40 co-administered with 1 mg of Aβ40. These results indicate

that the BBB permeabiliy of ^{125}I-PUT-Aβ40 is also saturable. Therefore, endogenous Aβ40 levels in the peripheral circulation of APP,PS1 animals, which were reported to increase linearly with age, could affect the BBB permeability of ^{125}I-PUT-Aβ40 to a similar extent as ^{125}I-Aβ40. Based on this information it is likely that a modest 1.5–2.0 fold higher PS value of ^{125}I-PUT-Aβ40 compared to ^{125}I- Aβ40 (Wengenack et al., 2000a) may, at the best, have a limited contribution to the differences in their plaque targeting abilities.

Our earlier work demonstrated that the accumulation of ^{125}I-Aβ40 in the extracellular space of APP,PS1 mouse brain is primarily influenced by the reduced clearance of Aβ40, mediated by metabolism and/or efflux, from the brain parenchyma (Kandimalla et al., 2005). Mouse brain slices containing cortex and hippocampus were used in this study as in vitro model to investigate the role of parenchymal metabolism and uptake on the differential plaque targeting ability of ^{125}I-Aβ40 and ^{125}I-PUT-Aβ40. This in vitro model has been used by several researchers to study the metabolism (Newman et al., 1990) and diffusion of ions (Newman et al., 1995), small (Gredell et al., 2004) and large molecules (Patlak et al., 1998) in the brain parenchyma. Uptake of ^{125}I-Aβ40 into WT mouse brain slices followed Michaelis-Menten kinetics, which suggested that the uptake is saturable. The inhibition of ^{125}I-Aβ40 uptake in WT mouse brain slices by metabolic inhibitors such as 2,4DNP and ouabain suggested that it is energy dependent and most likely carrier mediated. Preferential localization of F-Aβ40 in the brain parenchymal cells, most likely neurons, following a short incubation time (5 min) further confirms the presence of carrier mediated transport of Aβ40.

In contrast, the metabolic inhibitors such as 2,4DNP did not affect the uptake of ^{125}I-PUT-Aβ40 significantly, thereby, suggesting that the uptake of ^{125}I-PUT-Aβ40 in WT mouse brain slices is most likely by passive diffusion. Localization of F-PUT-Aβ40 in the extracellular space of the brain parenchyma but not in the cells provides further evidence that there is no receptor mediated uptake of PUT-Aβ40. The cellular uptake of Aβ40 in the brain parenchyma makes it unavailable for targeting the plaques located in the extracellular space. In contrast, PUT-Aβ40 is not taken up by the cells, remains in the extracellular space, and is available for binding to plaques, a desirable feature for imaging amyloid plaques.

In vitro fibril binding studies demonstrated that both ^{125}I-Aβ40 and ^{125}I-PUT-Aβ40 bind to Aβ40 fibrils with similar affinity (data not shown). However, the differences in the extracellular concentrations of the probe can alter plaque binding significantly. The extracellular concentration of ^{125}I-Aβ40 is not only reduced due to cellular uptake but also by the efflux and parenchymal metabolism. The degradation of ^{125}I-PUT-Aβ40 in the WT mouse brain slices was significantly lower than the previously reported degradation of ^{125}I-Aβ40 (Kandimalla et al., 2005). The efflux of ^{125}I-Aβ40 across WT mouse brain slices was found to be saturable and inhibited by 2,4-DNP (Kandimalla et al., 2005), thereby, suggesting that it is energy dependent and carrier mediated. The efflux of ^{125}I-PUT-Aβ40 on the other hand was much slower compared to that of ^{125}I-Aβ40 and was not dependent upon the donor concentration suggesting that it occurs via passive diffusion.

Despite its success in providing contrast enhancement of plaques following IV injection during MRI of APP, PS1 mouse brains ex vivo, the utility of PUT-Gd-Aβ40 for diagnostic use in animal models and patients is limited because:

a) carbodiimide-mediated modification of Aβ40 with putrescine is associated with problems inherent with the protein itself, such as crosslinking, aggregate and/or fibril formation, and insolubility.

b) PUT-Aβ40 forms fibrils more readily than Aβ40. The ease with which a molecule can form fibrils is considered as a direct measure of its likelihood to provide a seed for plaque formation.

Hence a new probe, Gd[N-4ab/Q-4ab]Aβ30, was produced as a putative MRI contrast enhancement agent by first synthesizing a glutamyl-4-aminobutane or asparagyl-4-aminobutane, which were then incorporated into the synthesis of the protein using standard solid phase methods (Poduslo et al., 2004). The complete chemical synthesis of this probe eliminates peptide crosslinking, aggregate and fibril formation, and insolubility that affected the carbodiimide-mediated modification of Aβ40 with putrescine. Apart from having the chemical purity, this probe is devoid of the neurotoxic domain found in Aβ40 and is not amyloidogenic like Aβ40. Additionally, Gd[N-4ab/Q-4ab]Aβ30 has good BBB permeability and labels neuritic plaques *in vitro* with affinity comparable to PUT-Aβ40. However, attempts to image amyloid plaques in APP,PS1 animals *in vivo* using this agent yielded only modest results. Studies are being conducted to enhance the *in vivo* efficacy of this probe through appropriate structural modifications to influence various physiological factors, parenchymal metabolism and

neuronal uptake, that were determined in the present study to adversely affect the plaque targeting ability.

In summary, these studies demonstrated that both ^{125}I-Aβ40 and ^{125}I-PUT-Aβ40 are rapidly eliminated from the systemic circulation following IV administration in WT animals. However, the peripheral pharmacokinetics of the probes did not significantly influence their plaque targeting capabilities. The higher concentration of endogenous Aβ40 in the peripheral circulation decreases the permeability of both compounds at the BBB. The metabolism of ^{125}I-PUT-Aβ40 is substantially lower in the brain slices compared to that of ^{125}I-Aβ40. This indicates that ^{125}I-PUT-Aβ40 is metabolically stable and may remain intact in the brain parenchyma with higher concentrations being available for plaque targeting than ^{125}I-Aβ40. Also, the rate of ^{125}I-PUT-Aβ40 efflux in WT brain slices was substantially lower compared to that of ^{125}I-Aβ40. Hence ^{125}I-PUT-Aβ40 tends to remain in brain parenchyma longer than ^{125}I-Aβ40. This study also demonstrates that the fluoresceine labeled Aβ40, but not ^{125}I-PUT-Aβ40, is taken up by cells, which makes the former unavailable for targeting the plaques located in the extracellular space. By comparing the distribution and metabolism of ^{125}I-Aβ40 and ^{125}I-PUT-Aβ40 following IV administration, it can be concluded that the inadequate targeting of ^{125}I-Aβ40 to amyloid plaques despite its carrier mediated uptake at the BBB could be due to cellular uptake, metabolism, and efflux of Aβ40 in the brain parenchyma. The knowledge gained from these studies will be very useful in the development of new Aβ derivatives with improved BBB permeability and plaque targeting.

ACKNOWLEDGEMENTS

We thank Dr. Dan McCormick and Jane A. Petersen for extending their technical expertise in synthesizing Aβ40; Dr. Karen Duff for the PS1 transgenic mouse line; Dawn Gregor for her excellent technical assistance; and Jennifer Scott for her excellent secretarial assistance.

REFERENCES

Agdeppa ED, Kepe V, Liu J, Flores-Torres S, Satyamurthy N, Petric A, Cole GM, Small GW, Huang SC and Barrio JR (2001) Binding characteristics of radiofluorinated 6-dialkylamino-2-naphthylethylidene derivatives as positron emission tomography imaging probes for beta-amyloid plaques in Alzheimer's disease. *J. Neurosci. Methods* **21**:RC189.

Bacskai BJ, Kajdasz ST, Christie RH, Carter C, Games D, Seubert P, Schenk D and Hyman BT (2001) Imaging of amyloid-beta deposits in brains of living mice permits direct observation of clearance of plaques with immunotherapy. *Nat. Neurosci.* **7**:369-372.

Dellian M, Yuan F, Trubetskoy VS, Torchilin VP and Jain RK (2000) Vascular permeability in a human tumour xenograft: molecular charge dependence. *Br. J. Cancer* **82**:1513-1518.

Gredell JA, Turnquist PA, Maciver MB and Pearce RA (2004) Determination of diffusion and partition coefficients of propofol in rat brain tissue: implications for studies of drug action in vitro. *Br. J. Anaesth.* **93**:810-817.

Kandimalla KK, Curran GL, Holasek SS, Gilles EJ, Wengenack TM and Poduslo JF (2005) Pharamacokinetic Analysis of the Blood-Brain Barrier Transport of 125I-A{beta}40 in Wild Type and Alzheimer's Disease Transgenic Mice (APP, PS1) and Its Implication for Amyloid Plaque Formation. *J. Pharmacol. Exp. Ther.*

Klunk WE, Engler H, Nordberg A, Wang Y, Blomqvist G, Holt DP, Bergstrom M, Savitcheva I, Huang GF, Estrada S, Ausen B, Debnath ML, Barletta J, Price JC, Sandell J, Lopresti BJ, Wall A, Koivisto P, Antoni G, Mathis CA and Langstrom B

(2004) Imaging brain amyloid in Alzheimer's disease with Pittsburgh Compound-B. *Ann Neurol* **55**:306-319.

Mackic JB, Bading J, Ghiso J, Walker L, Wisniewski T, Frangione B and Zlokovic BV (2002) Circulating amyloid-beta peptide crosses the blood-brain barrier in aged monkeys and contributes to Alzheimer's disease lesions. *Vas. Pharmacol.* **38**:303-313.

Maness LM, Banks WA, Podlisny MB, Selkoe DJ and Kastin AJ (1994) Passage of human amyloid beta-protein 1-40 across the murine blood-brain barrier. *Life Sci.* **55**:1643-1650.

Newman GC, Hospod FE and Patlak CS (1990) Kinetic model of 2-deoxyglucose metabolism using brain slices. *J. Chem. Doc.* **10**:510-526.

Newman GC, Hospod FE, Qi H, Patel H, Trowbridge SD and Patlak CS (1995) Effects of K+, pH and glutamate on 45Ca kinetics in hippocampal brain slices. *J. Neurosci. Nurs.* **59**:111-120.

Patlak CS, Hospod FE, Trowbridge SD and Newman GC (1998) Diffusion of Radiotracers in Normal and Ischemic Brain Slices. **18**:776-802.

Poduslo JF and Curran GL (1996a) Increased permeability of superoxide dismutase at the blood-nerve and blood-brain barriers with retained enzymatic activity after covalent modification with the naturally occurring polyamine, putrescine. *J. Neurochem.* **67**:734-741.

Poduslo JF and Curran GL (1996b) Polyamine modification increases the permeability of proteins at the blood-nerve and blood-brain barriers. *J. Neurochem.* **66**:1599-1609.

Poduslo JF, Curran GL, Haggard JJ, Biere AL and Selkoe DJ (1997) Permeability and residual plasma volume of human, Dutch variant, and rat amyloid beta-protein 1-40 at the blood-brain barrier.[see comment]. *Neurobiol. Dis.* **4**:27-34.

Poduslo JF, Curran GL, Peterson JA, McCormick DJ, Fauq AH, Khan MA and Wengenack TM (2004) Design and chemical synthesis of a magnetic resonance contrast agent with enhanced in vitro binding, high blood-brain barrier permeability, and in vivo targeting to Alzheimer's disease amyloid plaques. *Biochemistry* **43**:6064-6075.

Poduslo JF, Curran GL, Sanyal B and Selkoe DJ (1999) Receptor-mediated transport of human amyloid beta-protein 1-40 and 1-42 at the blood-brain barrier. *Neurobiol. Dis.* **6**:190-199.

Poduslo JF, Curran GL, Wengenack TM, Malester B and Duff K (2001) Permeability of proteins at the blood-brain barrier in the normal adult mouse and double transgenic mouse model of Alzheimer's disease. *Neurobiol. Dis.* **8**:555-567.

Poduslo JF, Wengenack TM, Curran GL, Wisniewski T, Sigurdsson EM, Macura SI, Borowski BJ and Jack CR, Jr. (2002) Molecular targeting of Alzheimer's amyloid plaques for contrast-enhanced magnetic resonance imaging. *Neurobiol. Dis.* **11**:315-329.

Skovronsky DM, Zhang B, Kung MP, Kung HF, Trojanowski JQ and Lee VM (2000) In vivo detection of amyloid plaques in a mouse model of Alzheimer's disease. *Proc. Natl. Acad. Sci. U.S.A.* **97**:7609-7614.

Wengenack TM, Curran GL and Poduslo JF (2000a) Targeting alzheimer amyloid plaques in vivo. *Nat. Biotechnol* **18**:868-872.

Wengenack TM, Whelan S, Curran GL, Duff KE and Poduslo JF (2000b) Quantitative histological analysis of amyloid deposition in Alzheimer's double transgenic mouse brain. *Neuroscience* **101**:939-944.

Zlokovic BV, Ghiso J, Mackic JB, McComb JG, Weiss MH and Frangione B (1993) Blood-brain barrier transport of circulating Alzheimer's amyloid beta. *Biochem. Biophys. Res. Commun.* **197**:1034-1040.

FOOTNOTES

*Present address: College of Pharmacy and Pharmaceutical Sciences, Florida A&M University, Tallahassee, FL 32307

Supported by NIH R01 AG22034 and NIH/NCRR/RCMI G12RR03020

FIGURE LEGENDS

Figure 1. Plasma pharmacokinetics of ^{125}I-Aβ40‡ (n=12) and ^{125}I-PUT-Aβ40 in 24 week old WT mice (n=3). Data are mean ± S.D; lines indicate the fit of the two-compartment pharmacokinetic model to the plasma concentration-time data; ‡from Kandimalla et al., 2005.

Figure 2. Degradation of ^{125}I-Aβ40‡ and ^{125}I-PUT-Aβ40 in various tissues obtained from 24 week old WT mice. Data are mean ± S.D. (n = 5); ‡from Kandimalla et al., 2005.

Figure 3. Effect of 1 mg (231 nM) of unlabeled Aβ40 co-administered intravenously with ^{125}I-PUT-Aβ40 (100 µCi) on the permeability surface area product (PS) and brain vascular volume (V_p) of ^{125}I-PUT-Aβ40 at the blood brain barrier in 24 week old WT mice. Each result represents the mean ± S.D. for three experiments. The differences between the PS values of control (^{125}I-PUT-Aβ40) and treatment (^{125}I-PUT-Aβ40 + Aβ40) was determined to be statistically significant ($p<0.05$) by two-way ANOVA followed by Bonferroni post-tests.

Figure 4. Effect of time on the uptake of ^{125}I-Aβ40 into 24 week old WT brain slices in vitro. Data are mean ± S.D (n = 5).

Figure 5. Effect of donor concentration on the uptake of ^{125}I-Aβ40 into 24 week old WT brain slices in vitro. Data are mean ± S.D (n = 5). Curves represent predictions of Michaelis-Menten type model fitted to the data.

Figure 6. Accumulation of Fluorescein labeled Aβ40 and Fluorescein labeled PUT-Aβ40 in the neurons and extracellular space of WT mouse brain slices in vitro, respectively (20X).

Figure 7. Effect of metabolic inhibitors on the uptake of ^{125}I-Aβ40 and ^{125}I-PUT-Aβ40 in 24 week old WT brain slices in vitro. Data are mean ± SD (n = 5); (*p<0.05, Student's t-test).

Figure 8. Effect of donor concentration on the efflux rates of ^{125}I- Aβ40 and ^{125}I-PUT-Aβ40 from 24 week old WT brain slices in vitro. Initial rates of efflux from the brain slices were normalized by the donor concentrations and plotted against log donor concentrations. Curve represents prediction of one-site competitive binding model using GraphPad Prism version 3.03.

Figure 9. CD spectra of ^{125}I- Aβ40 and ^{125}I-PUT-Aβ40 in PBS (pH = 7.2) at 4 ^{o}C

Figure 10. Kinetics of ^{125}I- Aβ40 and ^{125}I-PUT-Aβ40 fibril formation. THT binds to the β-sheet structure of the fibrils and emits fluorescence. The intensity of the fluorescence provides a direct measure of the extent of fibril formation.

JPET Fast Forward. Published on March 24, 2006 as DOI: 10.1124/jpet.105.095711
This article has not been copyedited and formatted. The final version may differ from this version.

Table 1. Comparison of the plasma pharmacokinetic parameters of ^{125}I-Aβ40 and ^{125}I-PUT-Aβ40 in 24 week WT mice

Parameters	^{125}I-Aβ40[1]	^{125}I-PUT-Aβ40	**p**
C_{max} (μCi/mL)	17.4 ± 2.7	8.6 ± 3.4	*
$T_{1/2}$ (α) (min)	0.9 ± 0.1	0.5 ± 0.1	**
$T_{1/2}$ (β) (min)	9.2 ± 2.3	8.9 ± 3.6	ns
Clearance (ml/min/g)	0.09 ± 0.02	0.23 ± 0.08	*
V_{SS} (ml/g)	0.9 ± 0.17	2.2 ± 0.7	*
AUC (min x μCi/mL)	50.5 ± 7.3	18.5 ± 7.0	**

Mean ± S.D (n=3); Statistical significance was indicated by *p<0.05 and **p<0.01 using Student's t-test; ns: non-significant p > 0.05;[1] from Kandimalla et al., 2005

JPET Fast Forward. Published on March 24, 2006 as DOI: 10.1124/jpet.105.095711
This article has not been copyedited and formatted. The final version may differ from this version.

Figure 1

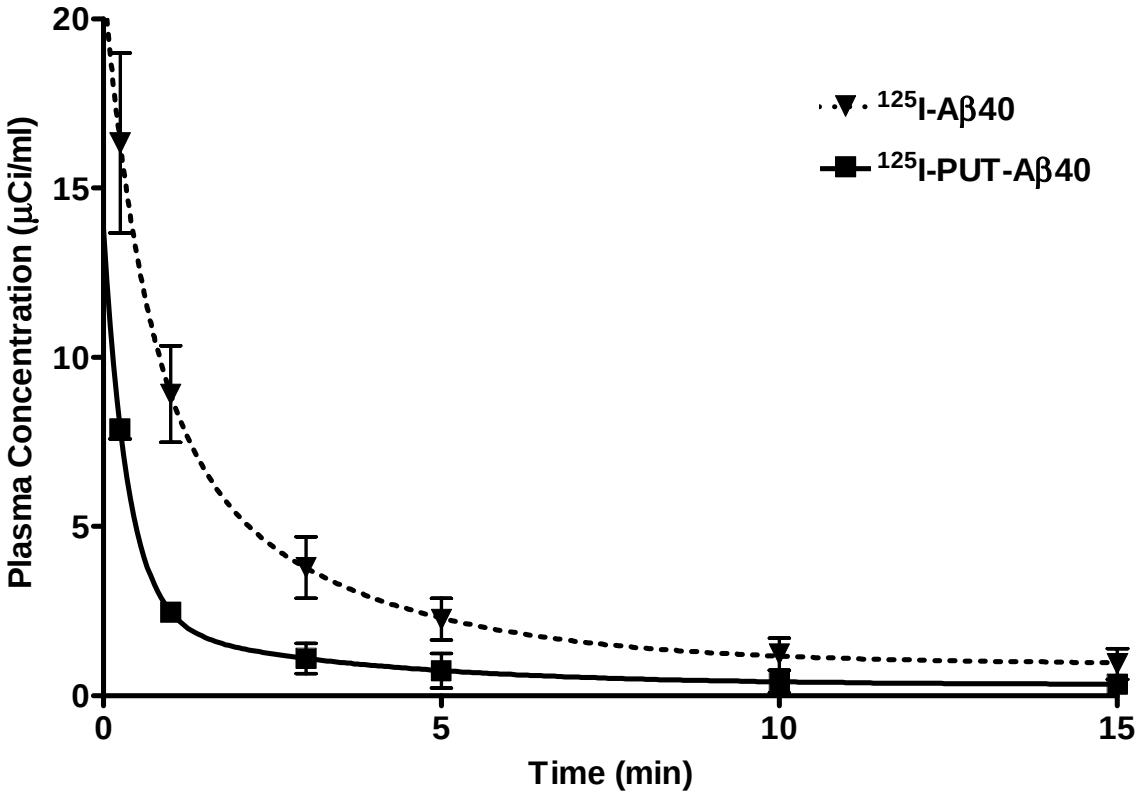

JPET Fast Forward. Published on March 24, 2006 as DOI: 10.1124/jpet.105.095711
This article has not been copyedited and formatted. The final version may differ from this version.

Figure 2

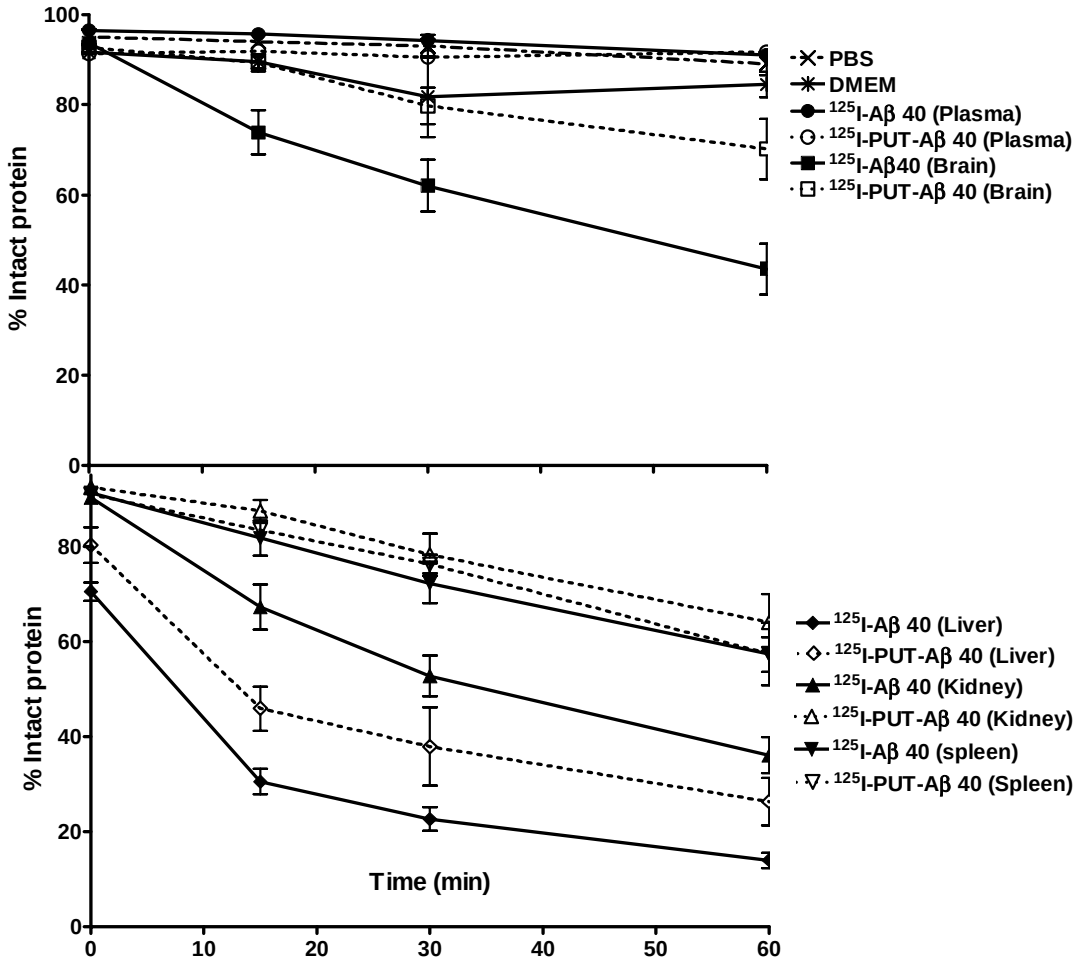

JPET Fast Forward. Published on March 24, 2006 as DOI: 10.1124/jpet.105.095711
This article has not been copyedited and formatted. The final version may differ from this version.

Figure 3

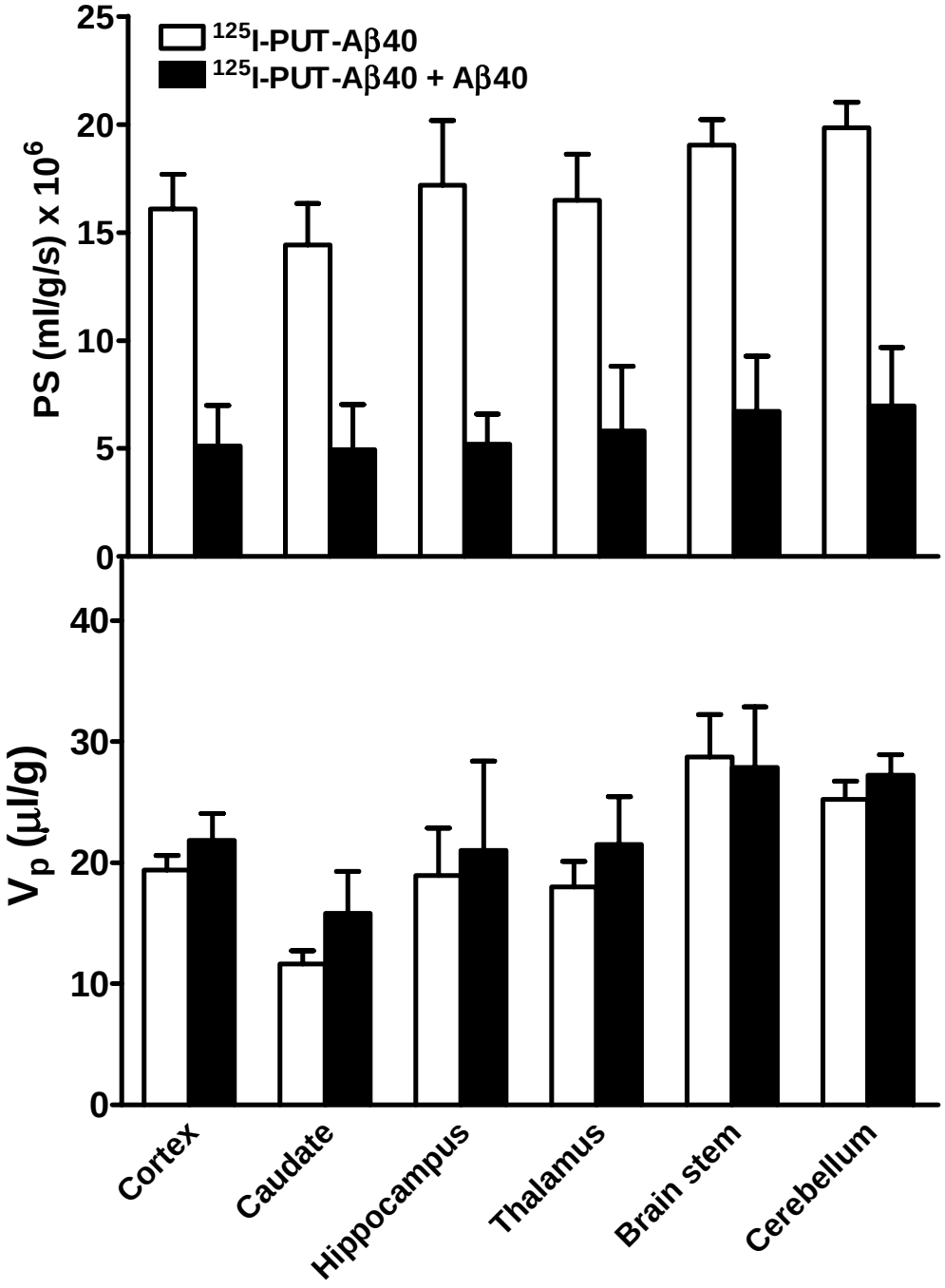

JPET Fast Forward. Published on March 24, 2006 as DOI: 10.1124/jpet.105.095711
This article has not been copyedited and formatted. The final version may differ from this version.

Figure 4

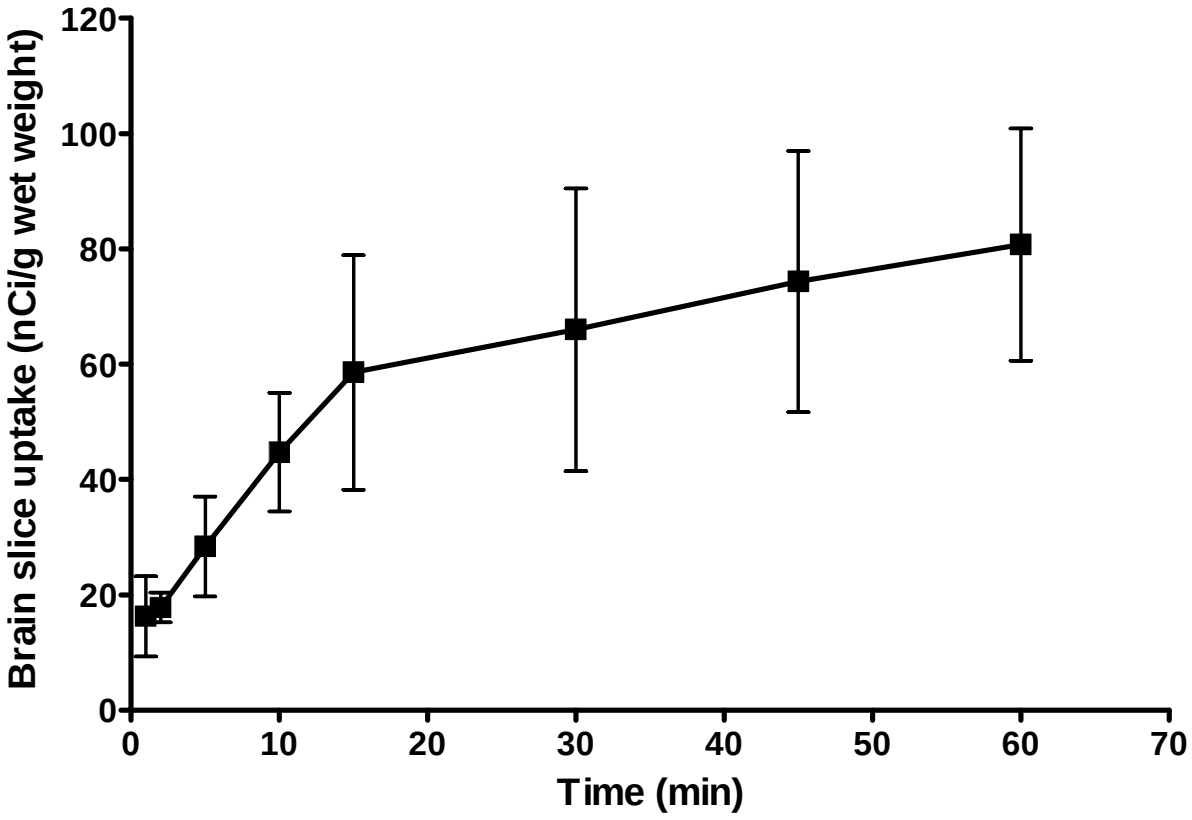

JPET Fast Forward. Published on March 24, 2006 as DOI: 10.1124/jpet.105.095711
This article has not been copyedited and formatted. The final version may differ from this version.

Figure 5

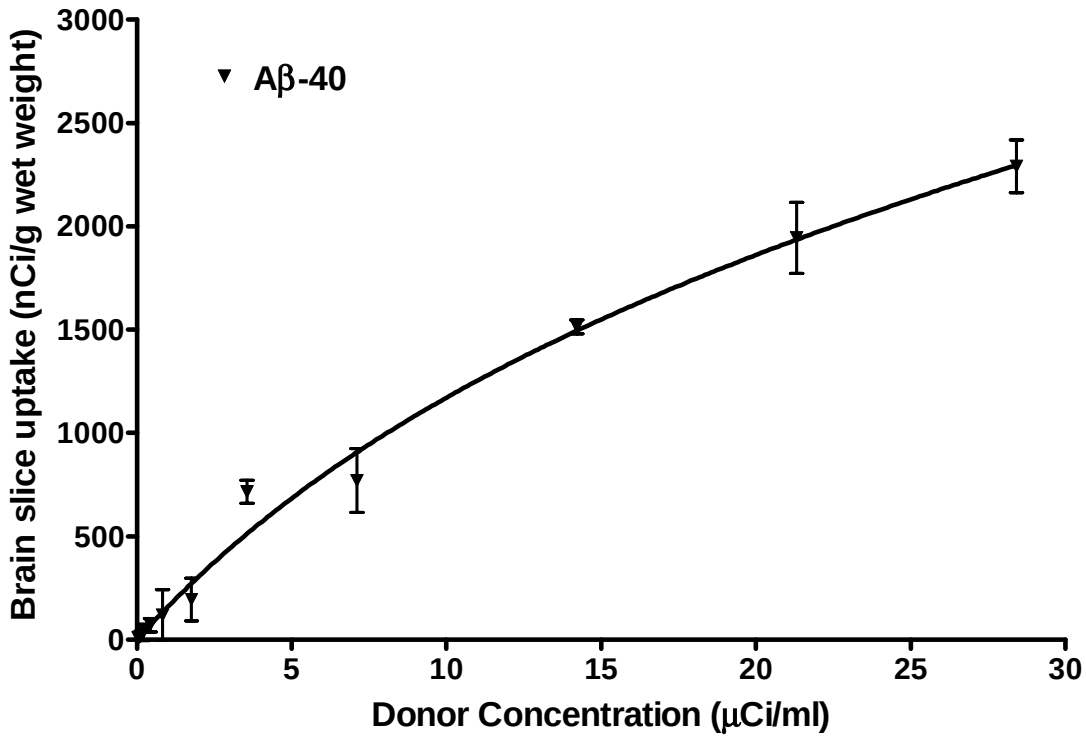

Figure 6

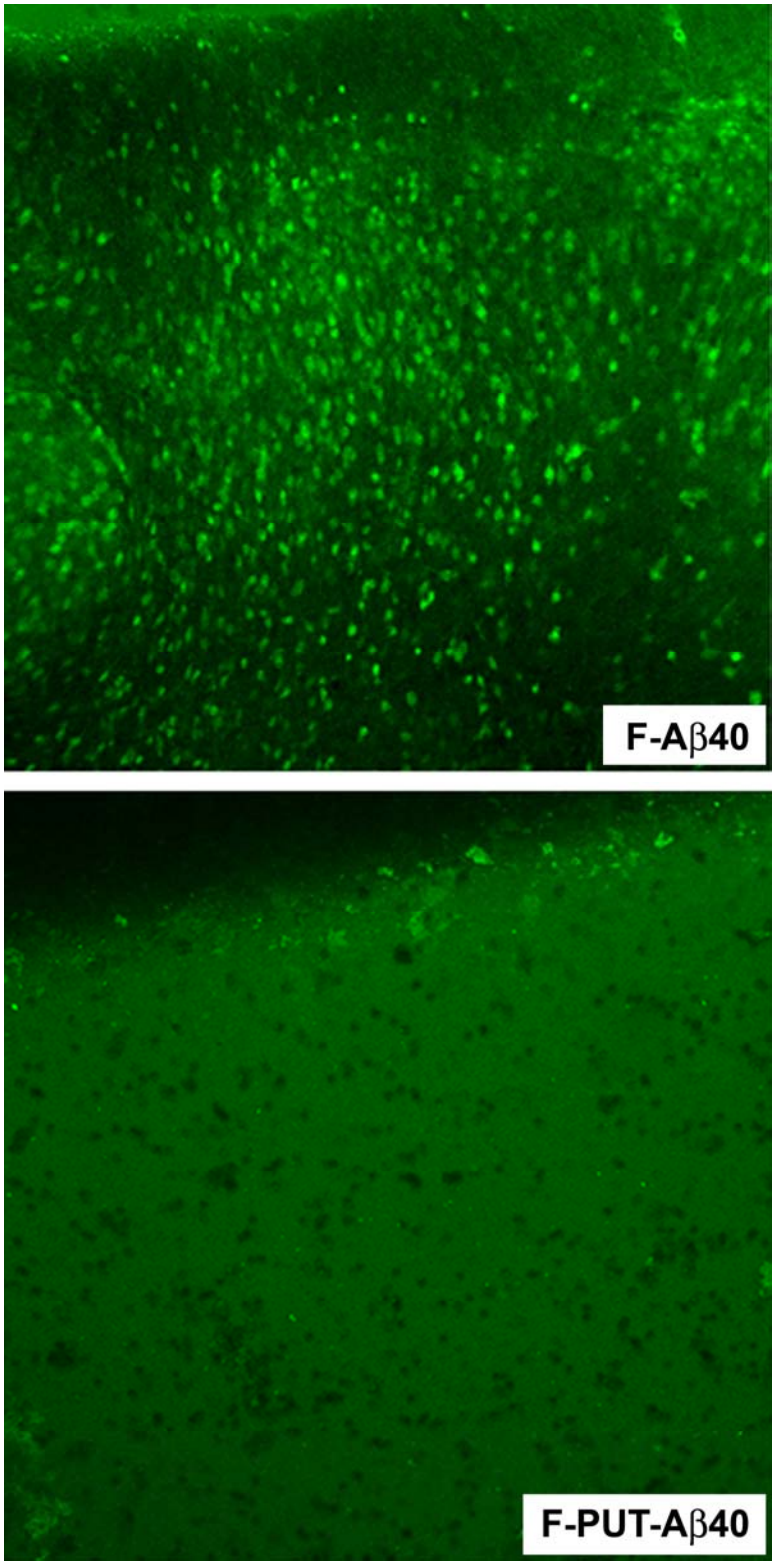

JPET Fast Forward. Published on March 24, 2006 as DOI: 10.1124/jpet.105.095711
This article has not been copyedited and formatted. The final version may differ from this version.

Figure 7

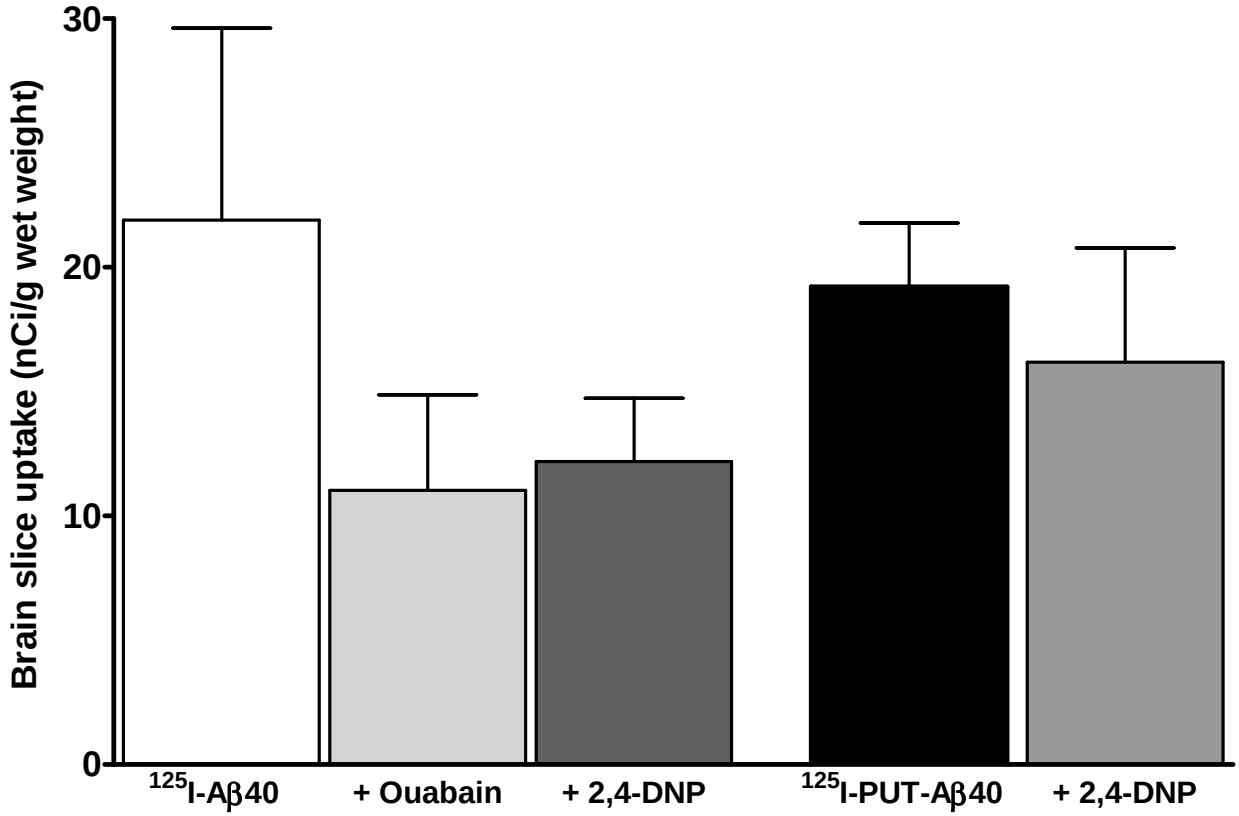

JPET Fast Forward. Published on March 24, 2006 as DOI: 10.1124/jpet.105.095711
This article has not been copyedited and formatted. The final version may differ from this version.

Figure 8

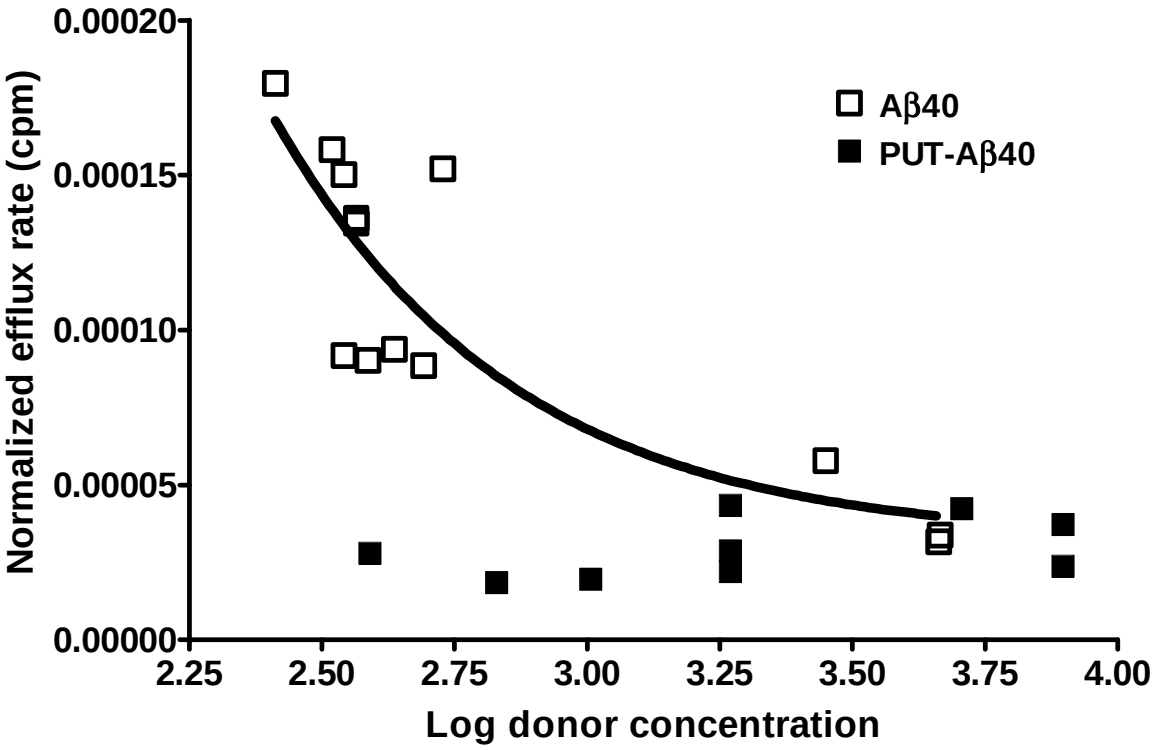

JPET Fast Forward. Published on March 24, 2006 as DOI: 10.1124/jpet.105.095711
This article has not been copyedited and formatted. The final version may differ from this version.

Figure 9

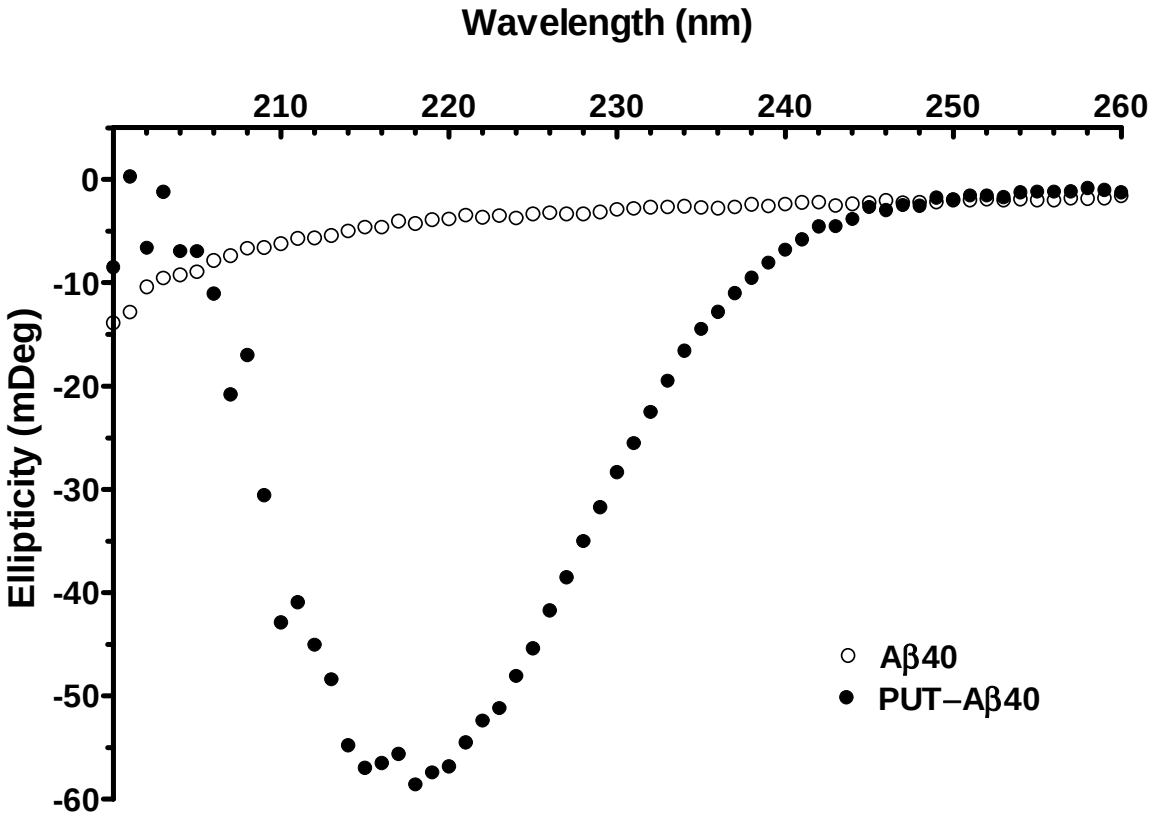

JPET Fast Forward. Published on March 24, 2006 as DOI: 10.1124/jpet.105.095711
This article has not been copyedited and formatted. The final version may differ from this version.

Figure 10